CALCULATIONS OF TRANSIENT FIELDS IN THE FELIX EXPERIMENTS AT ARGONNE USING HULL FIELD INTEGRATED TECHNIQUES

By

Kent R. Davey
School of Electrical Engineering
Georgia Institute of Technology
Atlanta, Georgia 30332-0250

Submitted to:

Argonne National Laboratory
4700 South Cass Avenue
Argonne, IL 60439

Final Report

Contract No. 31-109-ENG-38

September 30, 1985

ABSTRACT

The transient eddy current problem is characteristically computationally intensive. The motivation for this research was to realize an efficient, accurate, solution technique involving small matrices via an eigenvalue approach. Such a technique is indeed realized and tested using the null field integral technique. Using smart (i.e., efficient, global) basis functions to represent unknowns in terms of a minimum number of unknowns, homogeneous eigenvectors and eigenvalues are first determined. The general excitatory response is then represented in terms of these eigenvalues/eigenvectors. Excellent results are obtained for the Argonne Felix cylinder experiments using a 4 x 4 matrix. Extension to the 3-D problem (short cylinder) is set up in terms of an 8 x 8 matrix.

Introduction

Approaches to transient eddy current solutions to date tend to fall into one of two categories [4-7]:

(1) Time domain developed by forward difference albeit explicit or implicit. Spatial discretizations are pursued in much the same way as present time harmonic problems.

(2) Time domain developed via the characteristic eigenvalues/eigenvectors of the system. The spatial domain is characteristically pursued via either finite difference or finite element techniques.

The first approach is computationally intensive, involving the solution of the entire spatial domain recursively throughout the time period of interest. The second approach is theoretically more efficient, but is frought with many other problems. To obtain an accurate spatial discretization, one must necessarily employ a sufficiently large number of nodal points. For every modal point there will result an eigenvalue and related eigenvector. It is the author's experience that most real world problems have only a handful of dominant eigenvalues; by far most of the eigenvalues generated by a finite element technique are both spurious and (hopefully) subdominant. High accuracy in the spatial field representation is bought with the price of generating a host of important eigenvalues, a potential source of considerable error. It is with the intent of capitalizing on the positive features of the eigenvalue approach while minimizing the size of matrices (and thus number of eigenvalues) that the present research was undertaken.

The general theory involving the use of the null field integral equations in determining eigenvalues is first developed. The theory is applied to the Argonne Felix cylinder experiments [1-3]. Predictions are compared to the

exact analytical expressions for the problem. Extension of the technique to the short cylinder is discussed briefly, such an extension being realized through an 8 x 8 matrix rather than through the 4 x 4 matrix used for the long cylinder.

General Theoretical Development

The solution of the general matrix equation

$$\underline{X}' = \underline{\underline{A}}\,\underline{x} + \underline{b} \tag{1}$$

is found by first assuming

$$\underline{x} = e^{\lambda t} \tag{2}$$

and solving the homogeneous eigenvalue problem

$$\underline{\underline{A}}\,\underline{x} = \lambda\,\underline{x} \tag{3}$$

for eigenvalues $\underline{\underline{\lambda}}$ and eigenvectors $\underline{\underline{u}}$, where

$$\underline{\underline{\lambda}} = \begin{bmatrix} \lambda_1 & & & \\ & \lambda_2 & & \\ & & \ddots & \\ & & & \lambda_N \end{bmatrix}$$

$$\underline{\underline{u}} = \begin{bmatrix} \underline{x}_1 & \underline{x}_2 & \cdots & \underline{x}_N \end{bmatrix}$$

$\underline{x}_n$ = nth eigenvector

The temporal solution is written in terms of the particular solution $\underline{x}_p(t)$ as

$$\underline{x}(t) = \sum_{i=1}^{N} C_i \underline{x}_i e^{\lambda_i t} + \underline{x}_p(t) \ , \tag{4}$$

the C_i's being chosen to satisfy initial conditions.

Assuming temporal dependence $e^{-\lambda t}$ for all unknowns, the source-free magnetoquasistatic vector Helmholtz equation becomes

$$\nabla^2 \vec{A} + k^2 \vec{A} = 0 \tag{5}$$

where $k^2 = \lambda\mu\sigma$.

It is convenient from a pedagogical perspective to focus attention on the two dimensional object shown in Fig. 1, which has only a z-directed vector potential (the vector/subscript on $\vec{A}$ being henceforth dropped). The integral equation for A in each region can be written

$$\oint \left(\frac{\partial A_1'}{\partial n} G_1 - A_1' \frac{\partial G_2}{\partial n}\right) ds' = \begin{cases} A(r) & ; \ r \in \text{Domain 1} \\ A(r)/2 & ; \ r \text{ interface} \\ 0 & ; \ r \in \text{Domain 2} \end{cases} \tag{6}$$

$$-\oint \left(\frac{\partial A_2'}{\partial n} G_2 - A_2' \frac{\partial G_2}{\partial n}\right) ds' = \begin{cases} A(r) & ; \ r \in \text{Domain 2} \\ A(r)/2 & ; \ r \text{ interface} \\ 0 & ; \ r \in \text{Domain 1} \end{cases} \tag{7}$$

where

$G_1 = -\frac{j}{4} H_o^{(2)}(kr)$

$G_2 = -\ln(r)/2\pi$

$H_o^{(2)}$ = modified Hankel function of second kind, order zero.

Solution is realized by first assuming values for A_1 and $\partial A_1/\partial n$ in terms of a global basis set.

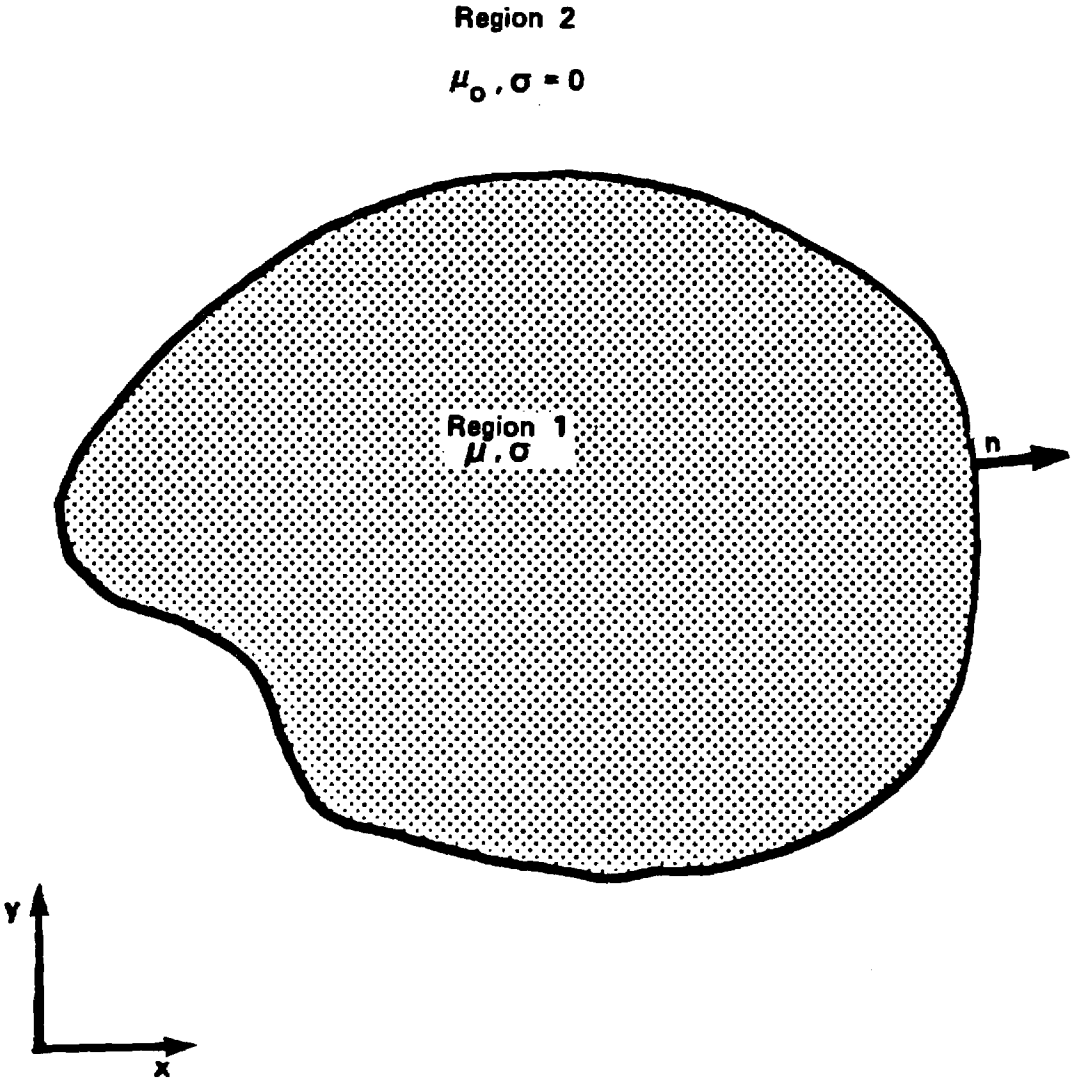

Figure 1. General two dimensional object characterized by a z - directed vector vector potential.

$$A_1 = \sum_{i=1}^{N} C_i \psi_i(\vec{r}) \tag{8}$$

$$\frac{\partial A_1}{\partial n} = \sum_{i=1}^{N} D_i \psi_i(\vec{r}) \tag{9}$$

(The basis functions in (8) and (9) will in general be identical but need not be for the analysis.) Boundary conditions on tangential $\vec{H}$ and normal $\vec{B}$ dictate that

$$A_1 = A_2 \tag{10}$$

$$\frac{1}{\mu} \frac{\partial A_1}{\partial n} = \frac{1}{\mu_o} \frac{\partial A_2}{\partial n} \tag{11}$$

so (8) and (9) characterize the problem entirely. The real advantage to the above approach comes about in the intelligent choice of $\psi_i(\vec{r})$. The more intelligent this choice, the smaller will be the determination matrix and thus the set of eigenvalues governing the problem. This choice can be adopted by analytical insight or experimental data taken, for instance, at $t = 0$, $t = t_{final}/2$, and $t = t_{final}$ (in which case $N = 3$).

Solution proceeds by arbitrarily choosing "N" points inside and outside the body. The "N" points outside the body are then used to write "N" null field equations using (6c) and the "N" points inside are used with (7c) to yield "N" more. These "2N" equations result in a matrix as follows:

$$\begin{bmatrix} -\int \psi_1 \frac{\partial G_1}{\partial n} & -\int \psi_2 \frac{\partial G_1}{\partial n} & \cdots & \int \psi_1 G_1 \\ \cdots & \cdots & \cdots & \cdots \\ \int \psi_N \frac{\partial G_2}{\partial n} & \cdots & -\int \psi_n \frac{\partial G_2}{\partial n} & \end{bmatrix} \begin{matrix} C_1 \\ \vdots \\ C_N \\ D_1 \\ \vdots \\ D_N \end{matrix} \equiv \underline{\underline{F}} \begin{matrix} \underline{C} \\ \underline{D} \end{matrix} = 0 \tag{12}$$

The eigenvalues of the system immediately drop out as those values of k for which the determinant of the matrix $\underline{\underline{F}}$ in (12) is zero. These must be found of several nonlinear root solving techniques (e.g., Newton Raphson, Secant, etc.). Once the zero determinant values of ($\underline{\underline{F}}$) are known, a new matrix $\underline{\underline{F}}$ can be defined

$$\underline{\underline{F}}' = \underline{\underline{F}} + \underline{\lambda} \tag{13}$$

The eigenvectors $\underline{u}$ of $\underline{\underline{F}}'$, and thus of the original system, can be obtained via several numerical packages (e.g., QR algorithm, Jacobi iteration, etc.). The interfacial unknowns for all time is written in terms of the system eigenvectors $\underline{x}_1, \underline{x}_2, \cdots, \underline{x}_{2N}$ and the eigenvalues $\lambda_1, \lambda_2, \cdots, \lambda_{2N}$ as

$$\begin{matrix} C_1 \\ \vdots \\ C_N \\ D_1 \\ \vdots \\ \\ D_N \end{matrix} = \begin{matrix} \underline{C} \\ \underline{D} \end{matrix} = \sum_{i=1}^{2N} g_i e^{\lambda_i t} \underline{x}_i + \underline{x}_p(t) \tag{14}$$

where the g_i's are obtained from initial conditions. Typically, the field inside a conductor is known at $t = 0^+$ (identical to that before the transient); $\underline{x}_p(t)$ is the normal steady state solution. The interfacial unknowns are easily determined using "N" equations from (6a) and "N" null field equations (7c) to give a matrix equation for initial unknowns which is <u>not</u> homogeneous.

The Felix Cylinder Experiments

The methodology is now implemented for a 2-D, three region problem (Fig. 2). The Felix cylinder experiments involved three cylinders, one of which will be examined here. The cylinder is slit down its length. At t = 0, an external vertical field is allowed to collapse with time constant τ = 39.68 msec. We wish to predict the self-generated fields for all time. There is in addition an externally applied z-directed field. As will be shown, the length is long enough that for measurements in the center of the cylinder (at z = 0), the finite length, horizontal slits, and z-directed external field have no effect on the self-excited x-y field. The infinite cylinder with no slits will show an indiscernible difference in eddy current field at z = 0. Finite length effects must be considered when L < π/first eigenvalue "k" (this is roughly when L ≈ 3 * diameter).

The solution proceeds as follows. First, recognize that the following basis set satisfies all boundary constraints on A

$$A(r = a) = C \sin \theta \tag{15}$$

$$\frac{\partial A}{\partial r}(r = a) = D \sin \theta \tag{16}$$

$$A(r = b) = E \sin \theta \tag{17}$$

$$\frac{\partial A}{\partial r}(r = b) = F \sin \theta \tag{18}$$

Next evaluate 4 null field equations

$$0 = \int_0^{2\pi} \left\{D \sin \theta \, G_1 - C \sin \theta \frac{\partial G_1}{\partial r}\right\} a \, d\theta \; ; \; r > a \tag{19}$$

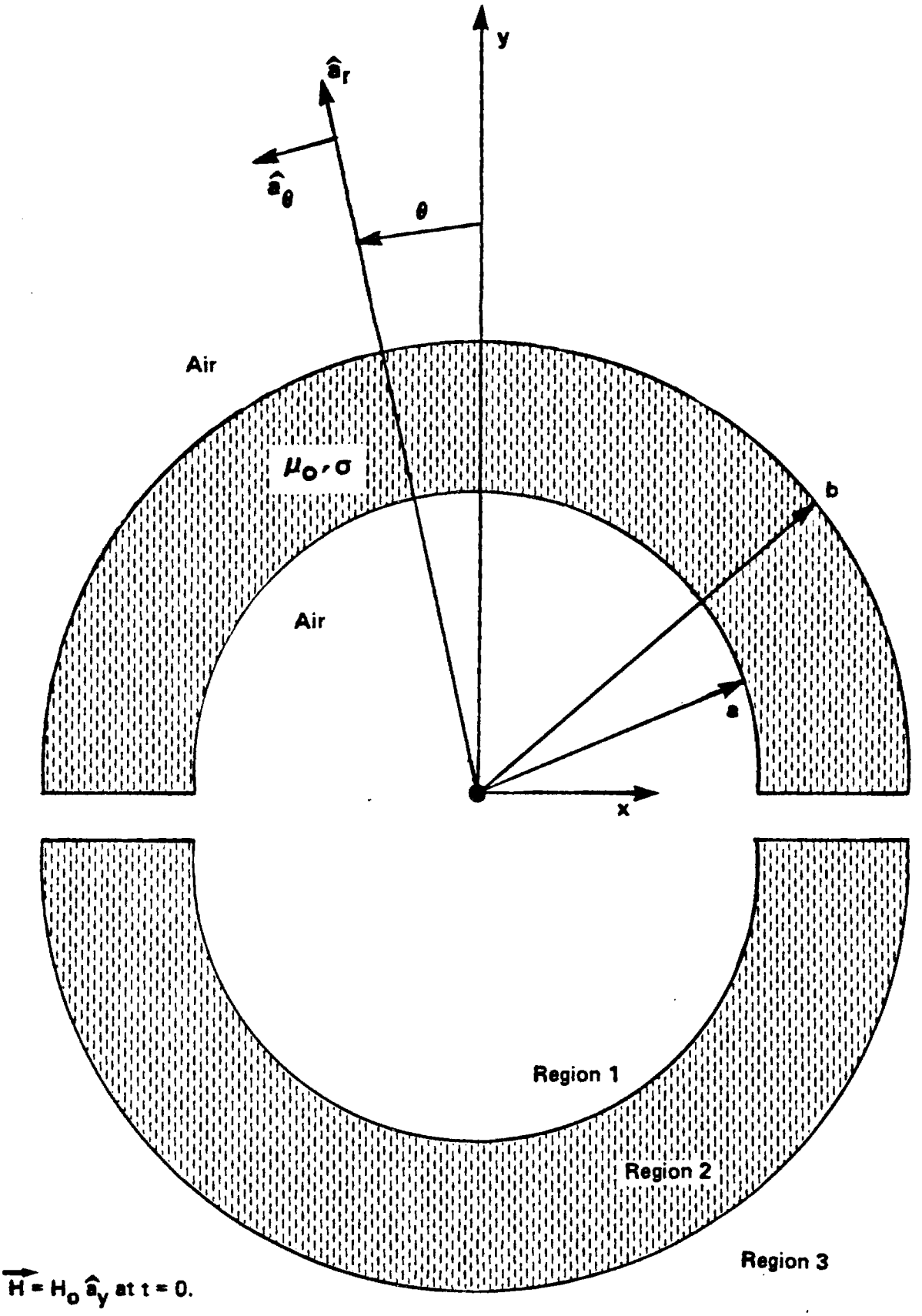

Figure 2. Felix Cylinder Experiment. Slit cylinder is immersed in a homogeneous field $\vec{H} = H_o \hat{a}_y$ at t = 0; a = 25.4mm, b = 50.8mm, length = 600mm, $\sigma = 2.538 \times 10^7$ mho/m; field collapses with time constant $\tau = 39.68$m sec.

$$0 = -\int_0^{2\pi} \left(D \sin\theta\, G_2 - C \sin\theta \frac{\partial G_2}{\partial r}\right) a\, d\theta$$

$$+ \int_0^{2\pi} \left(F \sin\theta\, G_2 - E \sin\theta \frac{\partial G_2}{\partial r}\right) b\, d\theta \; ; \; r < a \tag{20}$$

$$0 = -\int_0^{2\pi} \left(D \sin\theta\, G_2 - C \sin\theta \frac{\partial G_2}{\partial r}\right) a\, d\theta$$

$$+ \int_0^{2\pi} \left(F \sin\theta\, G_2 - E \sin\theta \frac{\partial G_2}{\partial r}\right) b\, d\theta \; ; \; r > b \tag{21}$$

$$0 = -\int_0^{2\pi} \left(F \sin\theta\, G_3 - E \sin\theta \frac{\partial G_3}{\partial r}\right) b\, d\theta \; ; \; r < b \tag{22}$$

where

$$G_1(r,r') = G_2(r,r') = -\frac{\ell n|\bar{r}-\bar{r}'|}{2\pi}$$

$$G_2(r,r') = -\frac{j}{4} H_o^{(2)}\left(k(r-r')\right)$$

$$k = \frac{\lambda}{\mu\sigma}$$

Note, it is necessary to avoid putting null field points along the $\theta = 0$ or $\theta = 180°$ axes or the origin where integration of sin θ terms identically yields zero. Otherwise no restraints are made. The system of equations (19)-(22) are written as the matrix

$$\begin{matrix} * & * & 0 & 0 & C \\ * & * & * & * & D \\ * & * & * & * & E \\ 0 & 0 & * & * & F \end{matrix} = 0 \tag{23}$$

The determinant of (23) is then evaluated for various values of k to determine zeros or eigenvalues. For the short cylinder dimension, as in Figure 2, the first three zeros were found to be 50.2830, 144.1659, 258.9145; a plot of the

determinant of (23) versus k is shown in Fig. 3 (along with the exact prediction which follows). The higher order eigenvalues are well removed from the base temporal decay; these higher order eigenvalues are reflective of the short temporal diffusion of the field across the thickness of the cylinder, a fact made more clear by looking at longer, thinner cylinders. For a medium sized cylinder with a = 57.14 mm, b = 69.85 mm, length = 600 mm, the eigenvalues k were found to be 51.4501, 257.9221, and 500.1842. A still larger cylinder with a = 131.7 mm, b = 136.5 mm, length = 1200 mm, gave eigenvalues k = 56.074, 659.2865, 1311.4041. Notice the increased separation between eigenvalues in each case reflective of the shorter relative diffusion time of the field through the cylinder walls.

As will be shown shortly, to predict the response to any external field drive, it suffices to determine the response to an external field H_o which drops instantaneously to zero; the final field being determined via convolution. Since the response field is dominated entirely by the first eigenvalue ($e^{\lambda_1 t}$), we need only predict C, D, E, and F at $t = 0^+$. At $t = 0^+$, only the field internal to the cylinder ($r < a$) is known to be equal to the value $H_o \hat{a}_y$ (or $A_z = H_o r \sin\theta$), the field at any other position being uncertain. The constants C, D, E, F follow by solving three null field equations in regions 2 and 3, and one inhomogeneous integral equation for region 1.

$$H_o r \sin\theta = \int_0^{2\pi} \left(D \sin\theta\, G_1 - C \sin\theta \frac{\partial G_1}{\partial r}\right) a\, d\theta \; ; \; r < a \tag{24}$$

$$0 = -\int_0^{2\pi} \left(D \sin\theta\, G_2 - C \sin\theta \frac{\partial G_2}{\partial r}\right) a\, d\theta$$

$$+ \int_0^{2\pi} \left(F \sin\theta\, G_2 - E \sin\theta \frac{\partial G_2}{\partial r}\right) b\, d\theta \; ; \; r < a \tag{25}$$

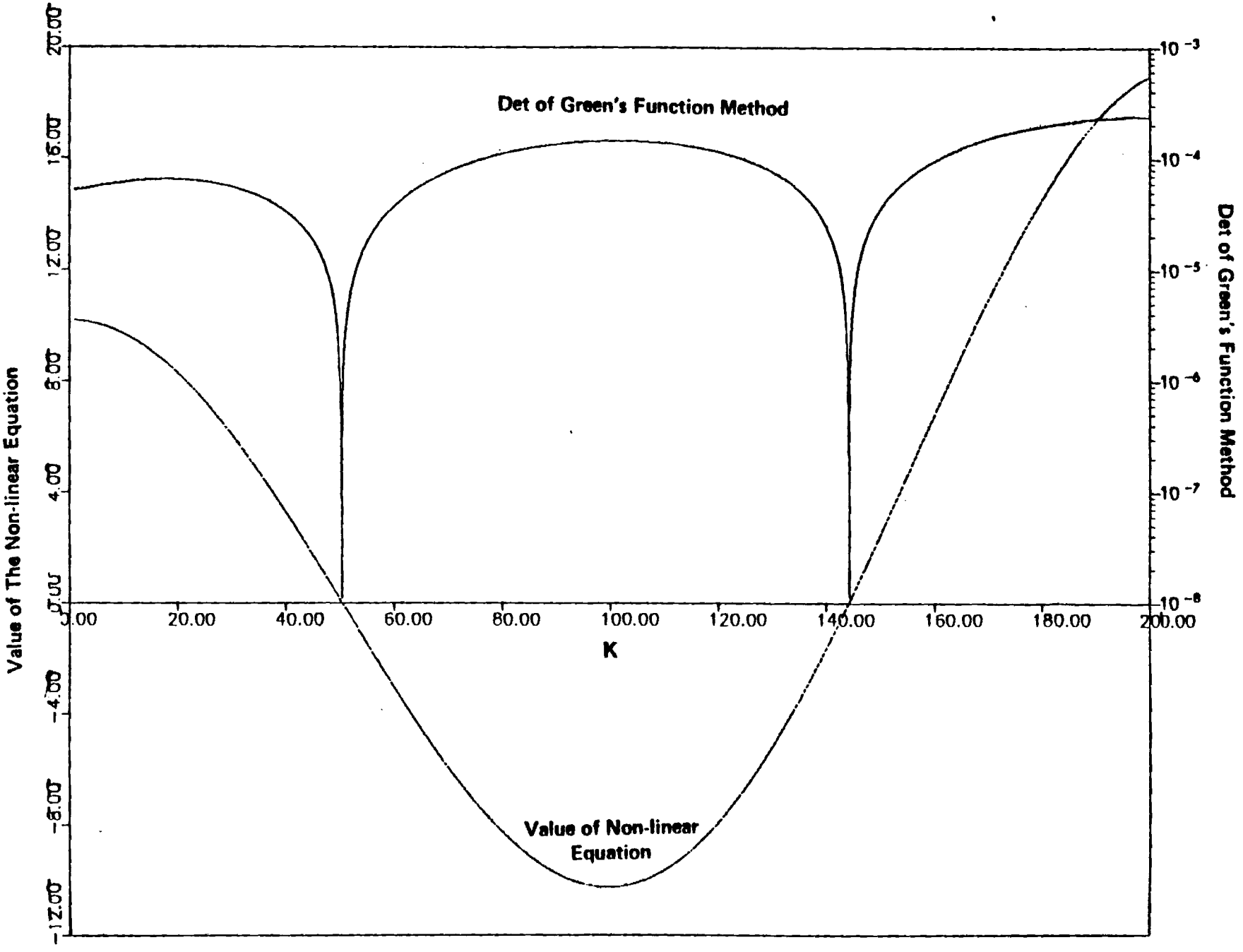

Fig. 3 Eigenvalues from Exact and Null-field Integral Calculations
Zeros of K are the Eigenvalues

$$0 = -\int_0^{2\pi} \left(D \sin\theta\, G_2 - C \sin\theta \frac{\partial G_2}{\partial r}\right) a\, d\theta$$

$$+ \int_0^{2\pi} \left(F \sin\theta\, G_2 - E \sin\theta \frac{\partial G_2}{\partial r}\right) b\, d\theta \;;\; r > b \qquad (26)$$

$$0 = -\int_0^{2\pi} \left(F \sin\theta\, G_3 - E \sin\theta \frac{\partial G_3}{\partial r}\right) b\, d\theta \;;\; r < b \qquad (27)$$

Once the constants are determined, the standard integral equations ((6a) and (7a)) yield the solution everywhere. This procedure has been implemented on a Cyber CDC; the results agree with those predicted by an exact solution to 5 decimal places (.001% error). These results are shown in the next section, where the exact solution is derived for comparison.

Analytical Formulation of the Eddy Current (Step Response) Field

In the exact analytical formulation possible in this test case, one begins by performing a separation of variables on $\nabla^2 A + k^2 A = 0$. The result for regions 1, 2, and 3 is

$$A_1 = Cr \sin\theta\, e^{-\frac{k^2}{\mu\sigma} t} \qquad (28)$$

$$A_2 = \left[AJ_1(kr) + BY_1(kr)\right] \sin\theta\, e^{-\frac{k^2}{\mu\sigma} t} \qquad (29)$$

$$A_3 = \frac{D}{r} \sin\theta\, e^{-\frac{k^2}{\mu\sigma} t} \qquad (30)$$

Enforcing the boundary conditions on A_2 and its normal derivative at $r = a$ and $r = b$ leads to an eigenvalue equation

$$[2J_1(kb) + kb(J_o(kb) - J_2(kb))][2Y_1(ka) - ka(Y_o(ka) - Y_2(ka))]$$
$$= [2J_1(ka) - ka(J_o/ka) - J_2(ka)][2Y_1(kb) + kb(Y_o(kb) - Y_2(kb))] \quad (31)$$

The numerical plot of (31) is shown in Fig. 3 to yield the same eigenvalues as those predicted by the integral technique.

By requiring the field internal to the cylinder to be H_o at $t = 0^+$ as above, we determine the constants A, B, C, D to be respectively (normalized to H_o)

Small Cylinder

A = 0.05899

B = 0.009081

C = 1

D = 0.001524

Medium Cylinder

A = 0.04878

B = 0.1281

C = 1

D = 0.004045

Large Cylinder

A = 0.2491

B = -0.3827

C = 1

D = 0.01798

These are again within 0.001% of the results found from the integral technique.

Total Transient Solution

So far we have found only the self-field due to the cylinder in response to step change in external field.

$$Hy = H_o - H_o u_{-1}(+) \tag{32}$$

The actual source field is

$$Hy = H_o - H_o u_{-1}(+) + H_o e^{-\alpha t} u_{-1}(+) \tag{33}$$

where

α = 39.68 msec.

The total response field is realized through a convolution of $(-dH_y/dt)$ with $e^{-\lambda t}$, i.e.,

$$\begin{aligned} H_{response} &= \int_0^t \left(-\frac{d}{dt}(H_y)_{t=\tau}\right) e^{-(t-\tau)} d\tau \\ &= \int_0^t \alpha H_o e^{-\alpha\tau} e^{-\frac{k^2}{\mu\sigma}(t-\tau)} d\tau \\ &= \frac{\alpha e^{-\frac{k^2}{\mu\sigma}t}}{\frac{k^2}{\mu\sigma} - \alpha} \left(e^{(\frac{k^2}{\mu\sigma} - \alpha)t} - 1\right) \end{aligned} \tag{34}$$

The total field is found as the response field (34) plus the source field $H_o e^{-\alpha t} \hat{a}_y$. Recalling that $H_r = \frac{1}{r}\frac{\partial A_z}{\partial \theta}$ and $H_\theta = -\frac{\partial A_z}{\partial r}$, it is a simple matter to construct the following solution table (Table I) for the total field. A plot of the response field and total field in region 2 (or 3) at r = b of the small cylinder is shown in Figs. 4 and 5 (H_r and H_θ).

The reader should note that the cylinder current density $\underline{J} = -\nabla^2 \underline{A}$ does not change its spatial character with time unless secondary and tertiary eigenvalues are significant in the problem. The current distribution through-

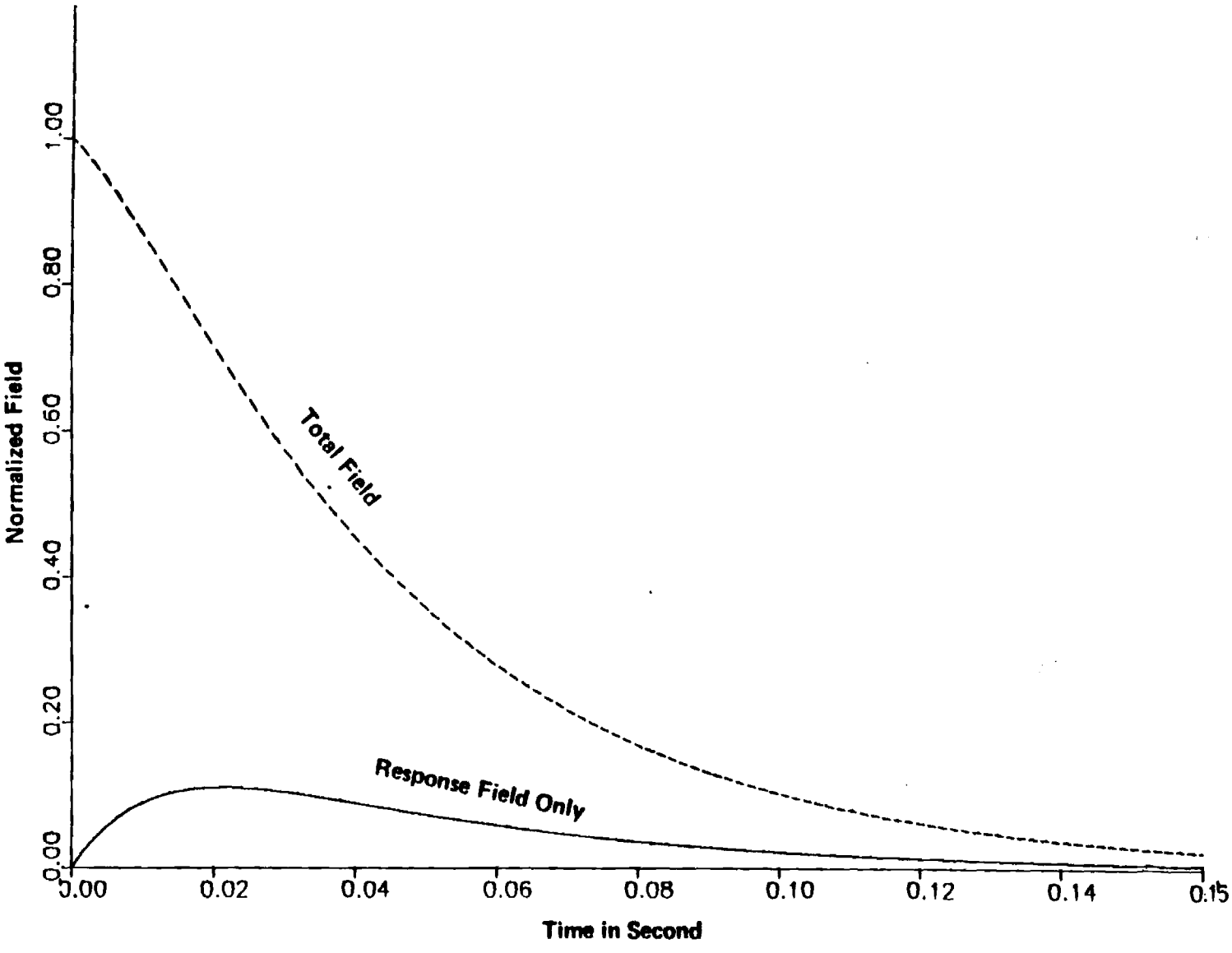

Fig. 4 R Component of Region(2) at Outer Radius

Outer Diameter 0.1016 meter, Thickness 0.0254 meter

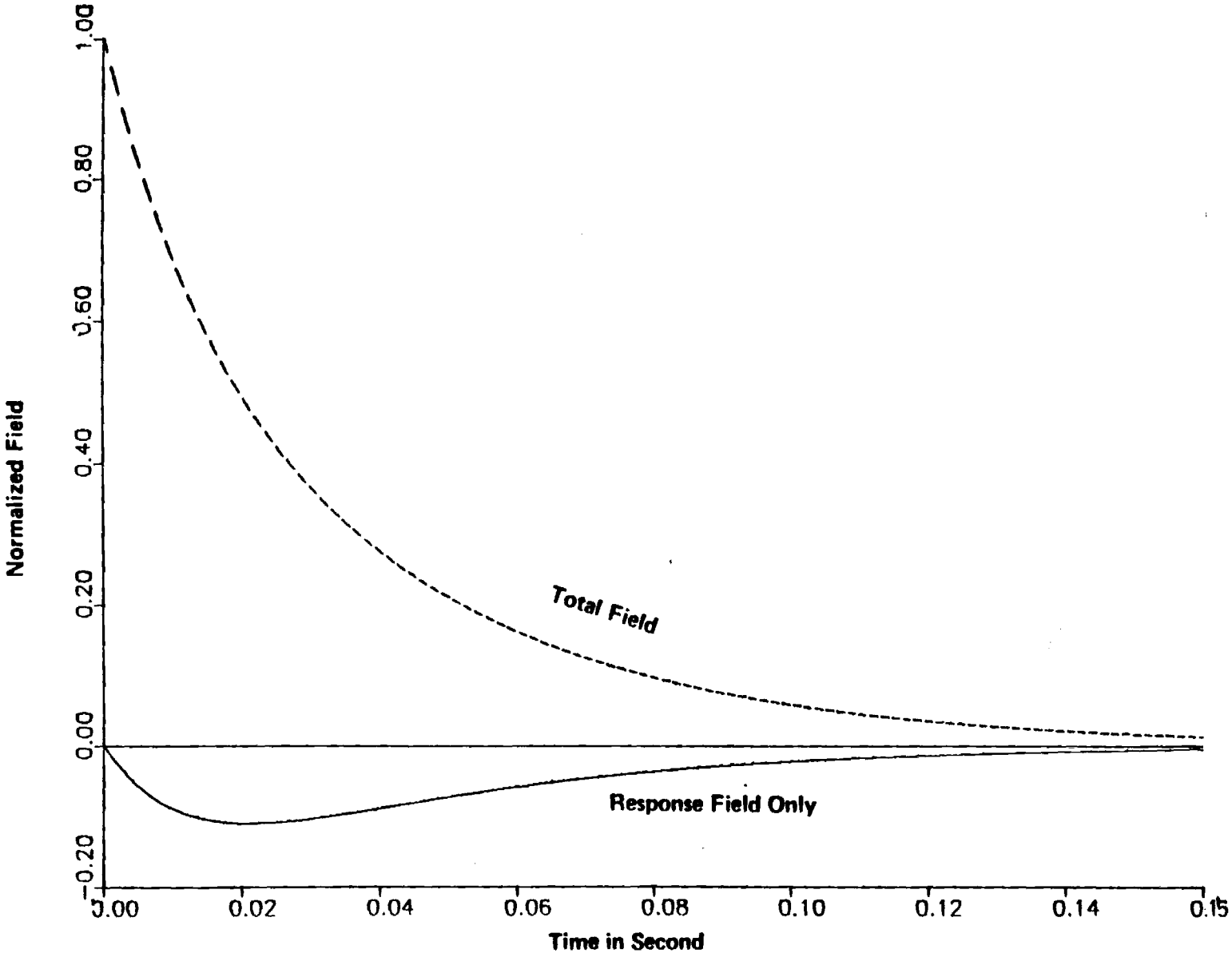

Fig. 5 Theta Component of Region(2) at Outer Radius

Outer Diameter 0.1016 meter, Thickness 0.0254 meter

Table 1. Total H field Response in the Cylinder

Component	Region	H
H_r	(1)	$H_o \cos\theta \left(e^{-\alpha t} + T(t)\right)$
	(2)	$H_o \cos\theta\, e^{-\alpha t} + \frac{H_o}{r}\left[AJ_1(kr) + BY_1(kr)\right]\cos\theta\, T(t)$
	(3)	$H_o \cos\theta\, e^{-\alpha t} + \frac{H_o D}{r^2}\cos\theta\, T(t)$
H_θ	(1)	$-H_o \sin\theta \left[e^{-\alpha t} + T(t)\right]$
	(2)	$-H_o \sin\theta \left(e^{-\alpha t} - \left[\frac{kA}{2}\left(J_o(kr) - J_2(kr)\right)\right.\right.$ $\left.\left. + \frac{kB}{2}\left(Y_2(kr)_o - Y_2(kr)\right)T(+)\right]\right)$
	(3)	$-H_o \sin\theta \left[e^{-\alpha t} - \frac{D}{r^2}T(t)\right]$

where $T(t) = \alpha \dfrac{e^{-\frac{k^2}{\mu\sigma}t}}{\left(\frac{k^2}{\mu\sigma} - \alpha\right)}\left(e^{\left(\frac{k^2}{\mu\sigma} - \alpha\right)t} - 1\right)$

out the cylindrical annulus is depicted in Fig. 6 by x's and o's whose size is indicative of the current density strength. Fig. 7 gives a more analytical picture of the current density radial distribution for θ = 0°, 22.5°, 45°, 67.5°, and 90°.

The large (R = 136.5 mm) and medium (R = 69.8 mm) cylinder eigenvalues are shown in Figs. 8 and 9; plotted in each is the analytical expression (31). These zeros agree to five decimal places with those predicted from the integral technique. Figures 10 and 11 show the large cylinder predicted versus experimental B_z fields for the total and induced fields, respectively. The dots indicate field data measured at the center of the cylinder. Figures 12 and 13 show the same B_z fields for the medium cylinder. The dots, however, are B_z field data 20 cm along the axis of the cylinder. These data points would be expected to be only slightly lower than those at the center. The agreement in all four curves is very reasonable.

Finite Length Effects

A first refinement taken to account for finite length effects is obtained by reconsidering the governing equation, $\nabla^2 A - \mu\sigma \frac{\partial A}{\partial t} = 0$. As before, we first separate into space and time, letting

$$A_z = U(\vec{r})e^{-\lambda t} = R(r)Z(z)\Theta(\theta)e^{-\lambda t}$$

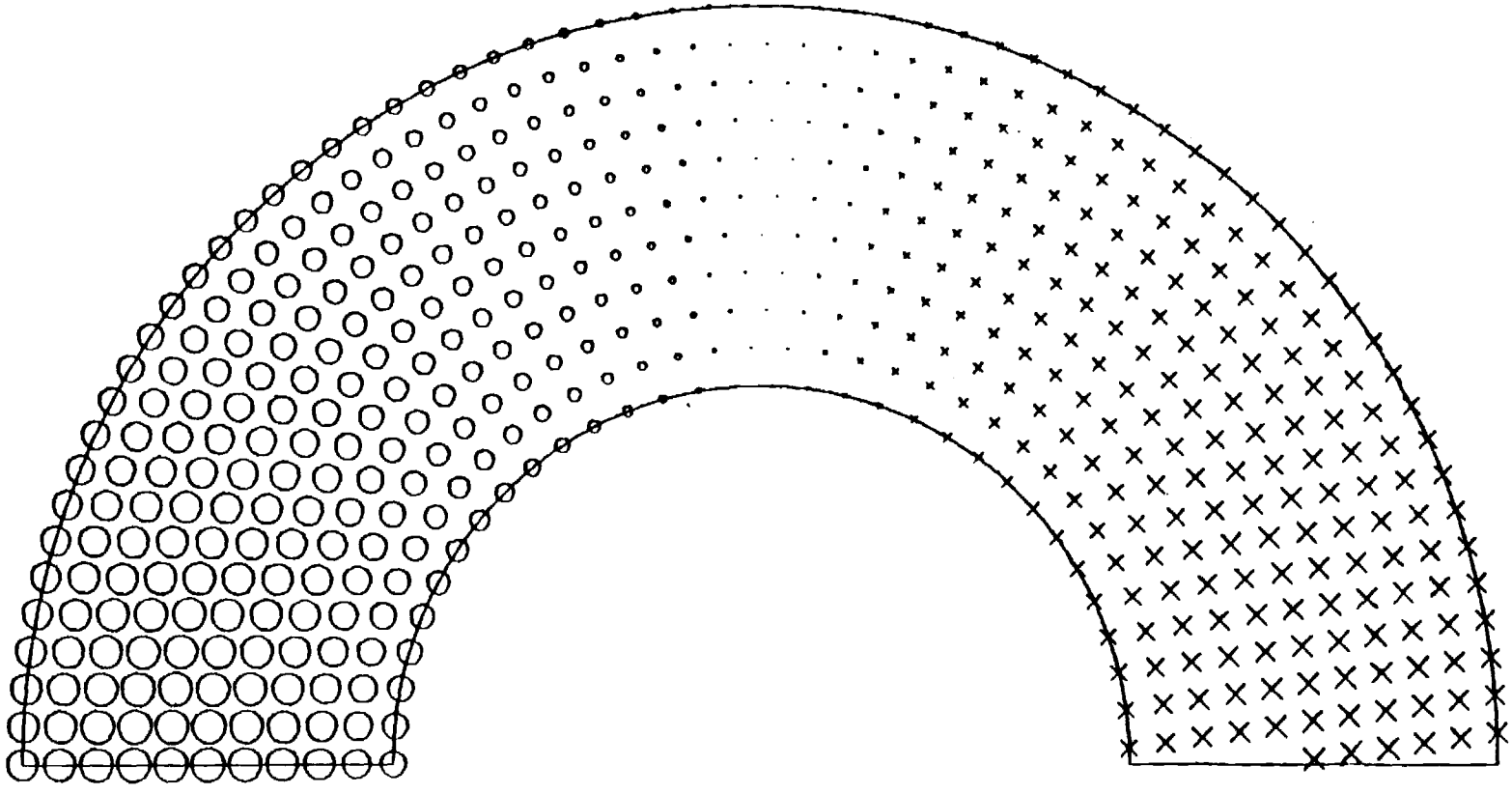

Fig. 6 Distribution of Current in the Annular Region

Magnitude of Current Density is Represented by the Size of X—O

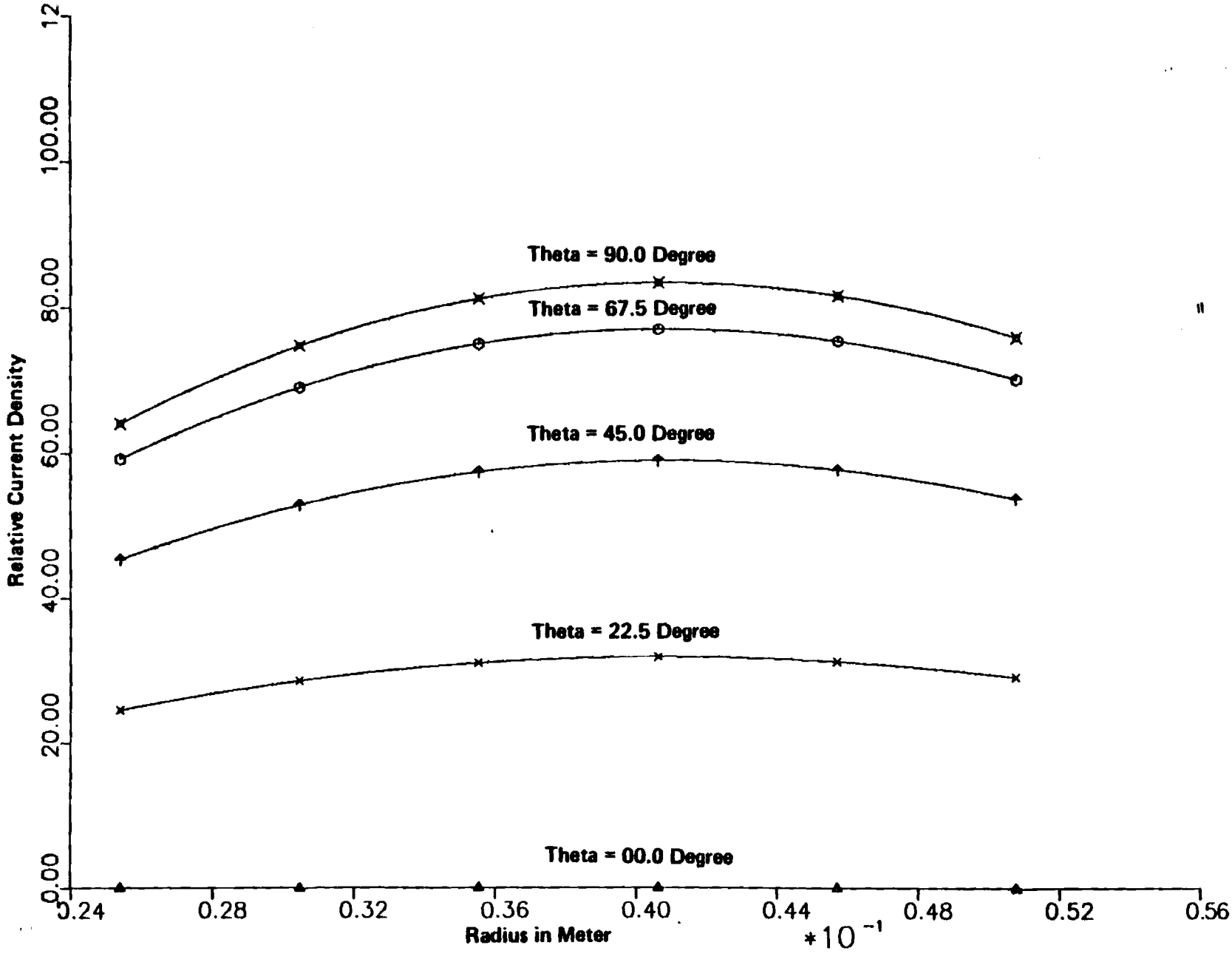

Fig. 7 **Distribution of Current**

Outer Diameter 0.1016 m, Thickness 0.0254 m

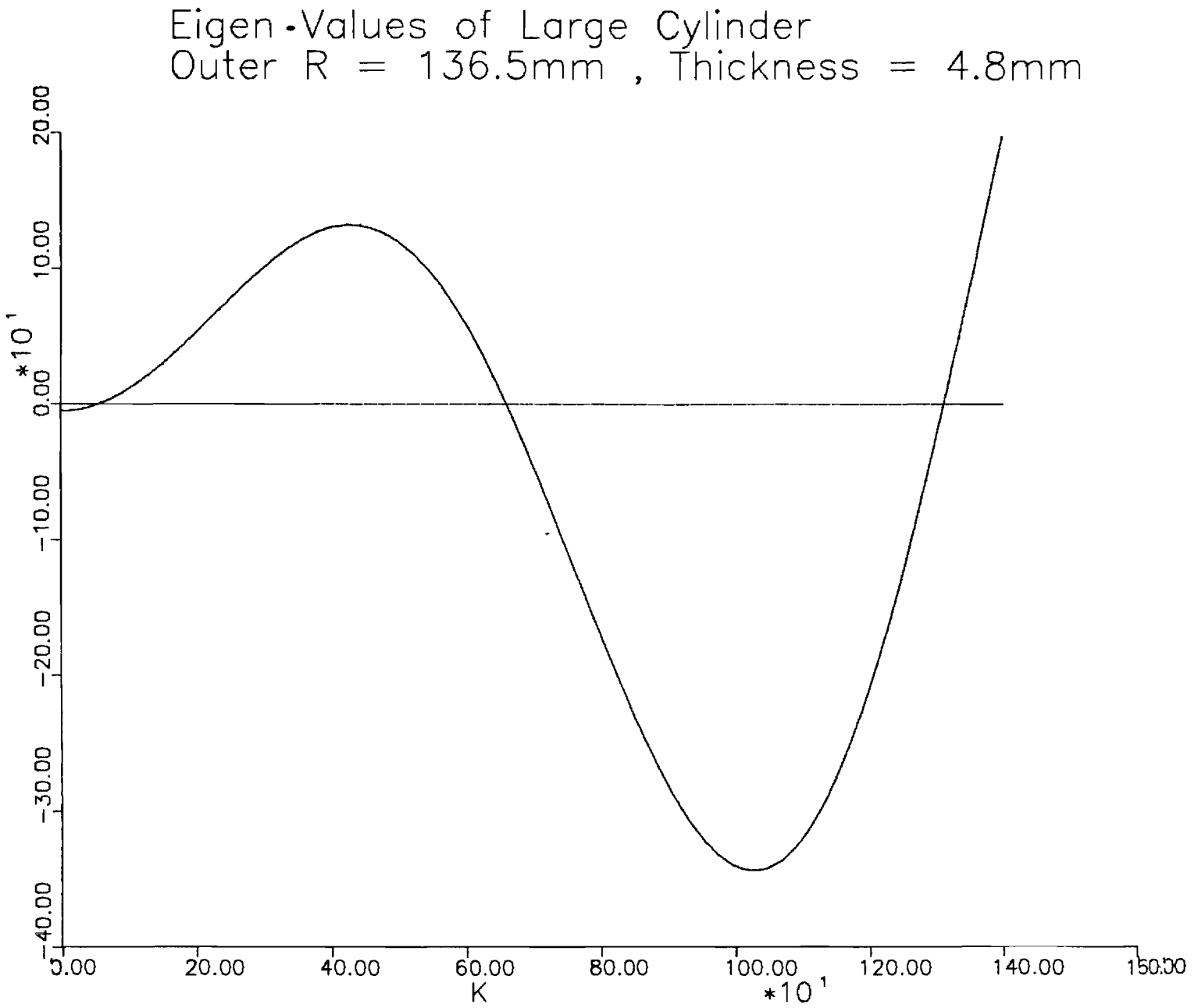

Fig. 8 Plot Eq.(31) versus k; the zero crossings show the eigenvalues expected for the large cylinder.

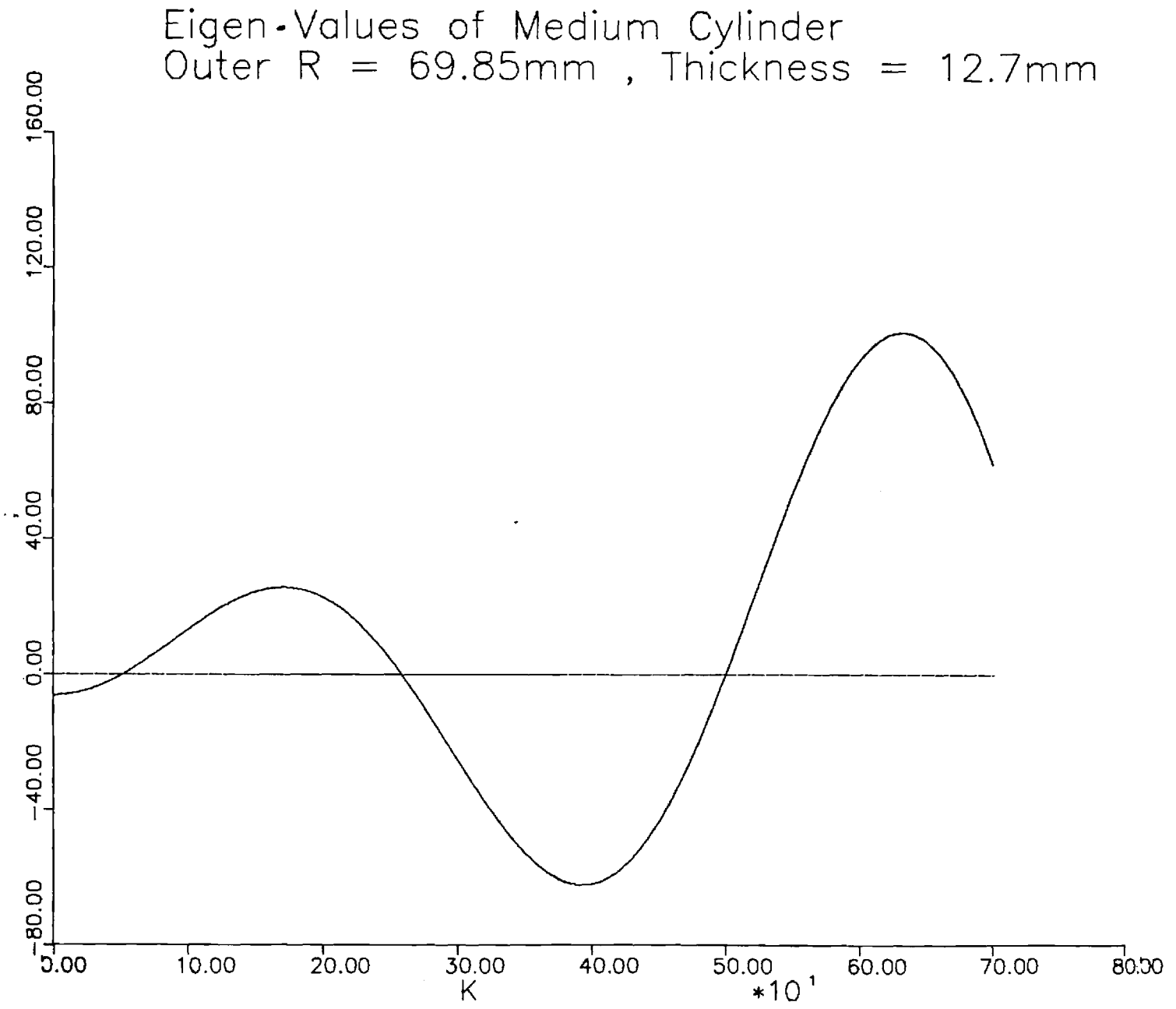

Fig. 9 Plot of Eq.(31) versus k for the medium cylinder; the zero crossings indicate the eigenvalues.

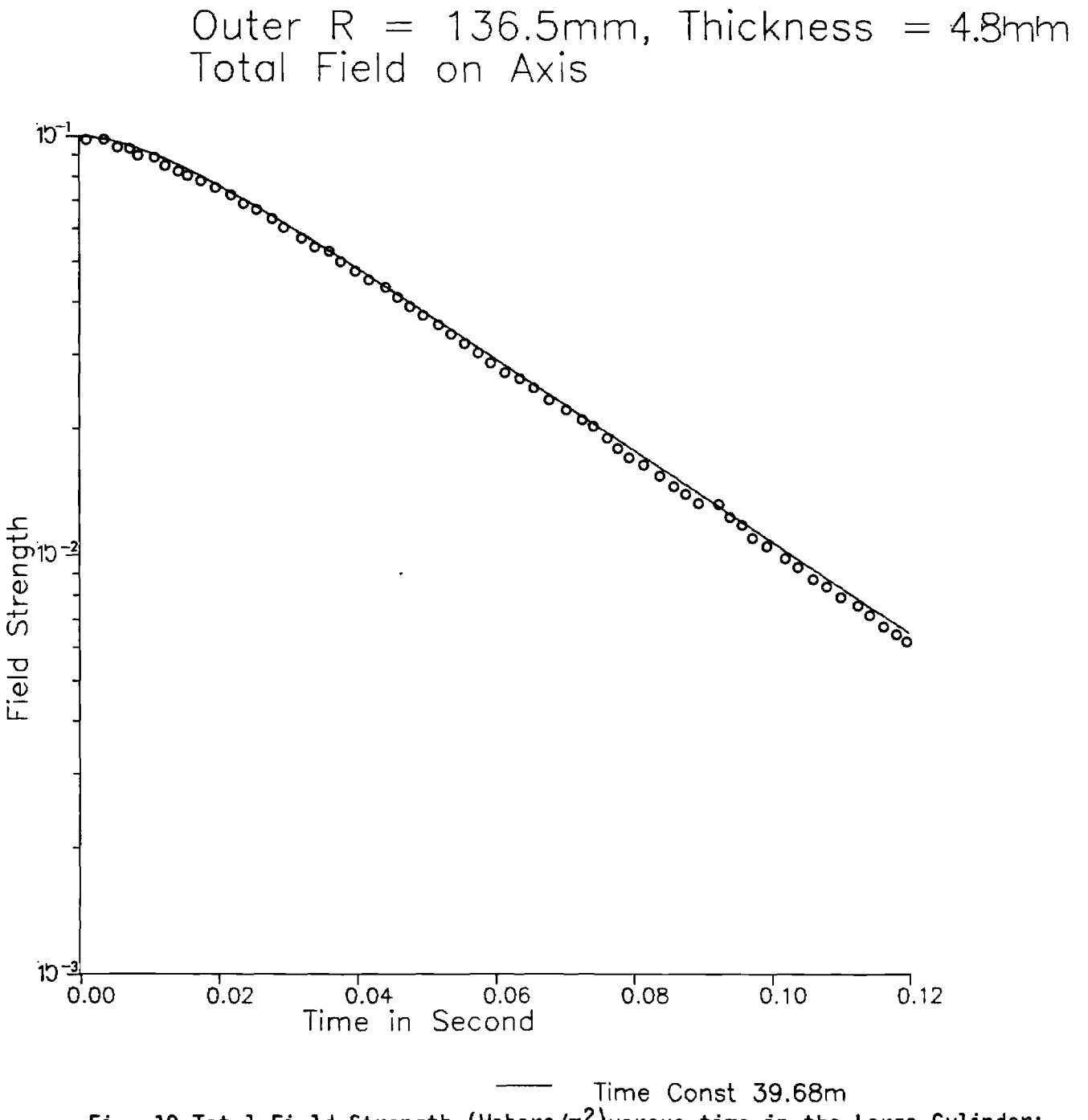

Fig. 10 Total Field Strength (Webers/m^2)versus time in the Large Cylinder; external field constant 39.68 msec. The dots indicate experimental values at the center of the cylinder.

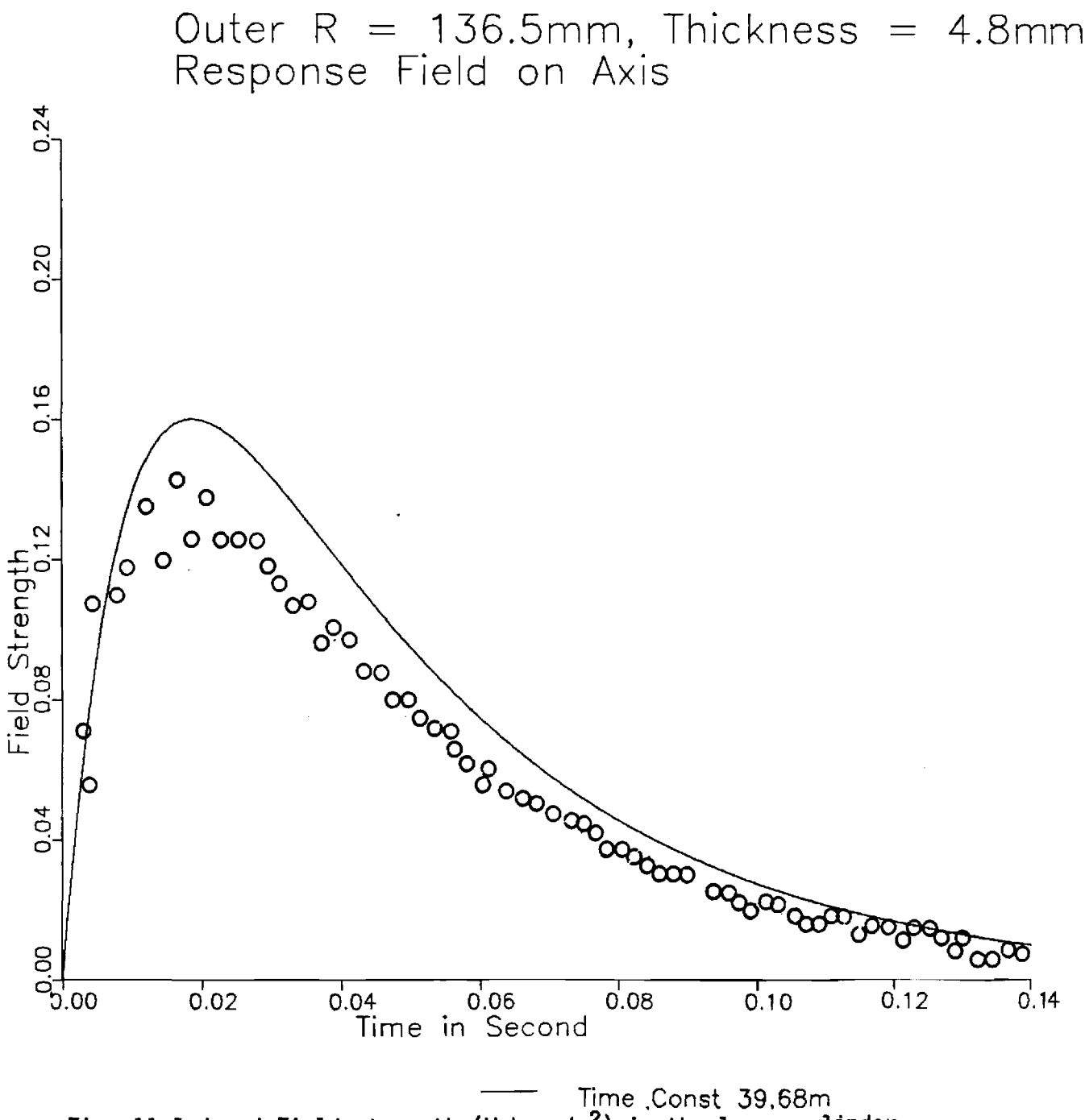

Fig. 11 Induced Field strength (Webers/m^2) in the large cylinder versus time; main field time constant is 39.68 msec. Dots indicate experimental data at the center of the cylinder.

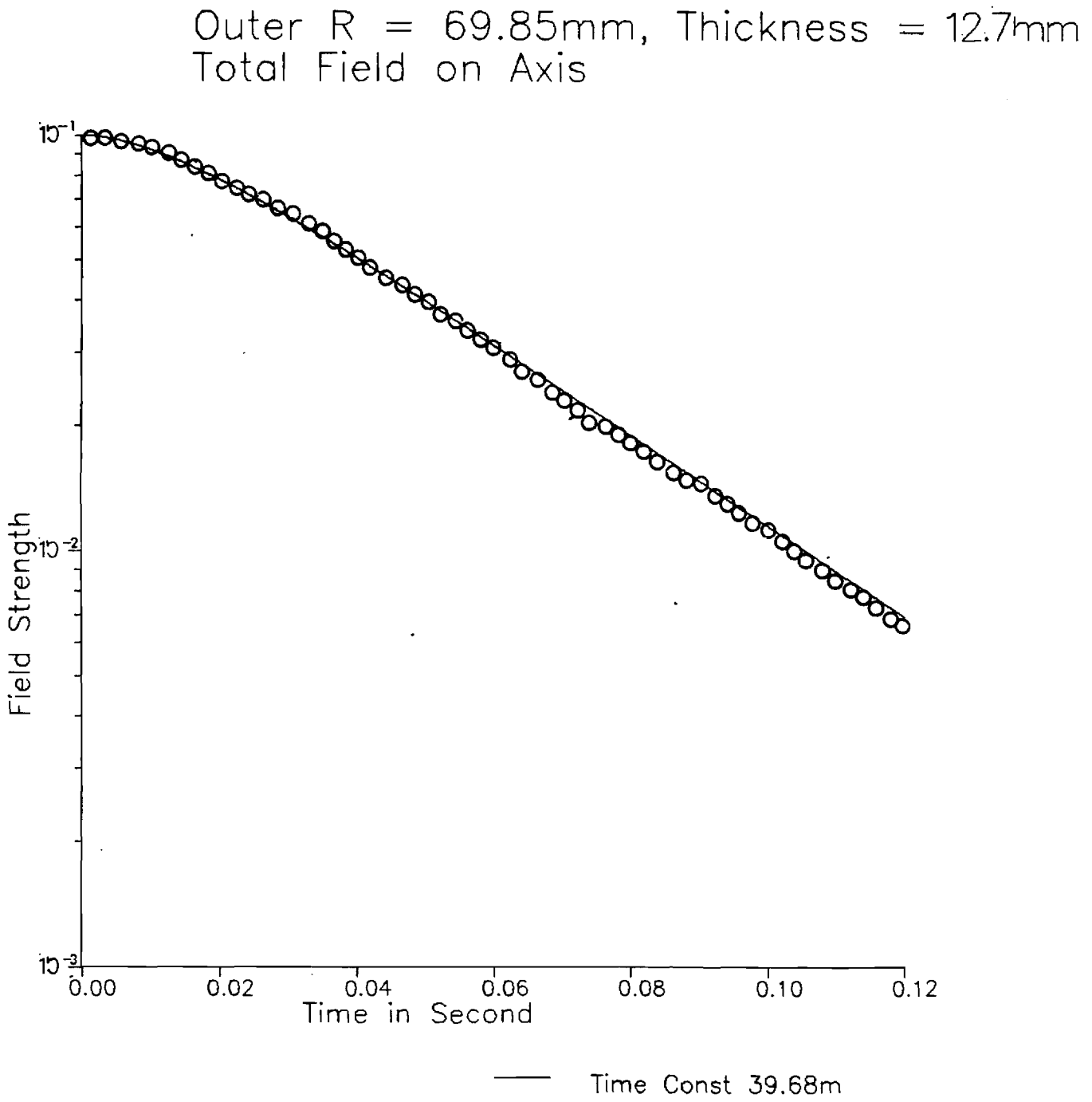

Fig. 12 Total Field response (Webers/m^2) versus time in the medium cylinder; main field time constant is 39.68. Dots indicate experimental data 20 cm from the center of the cylinder along the z axis.

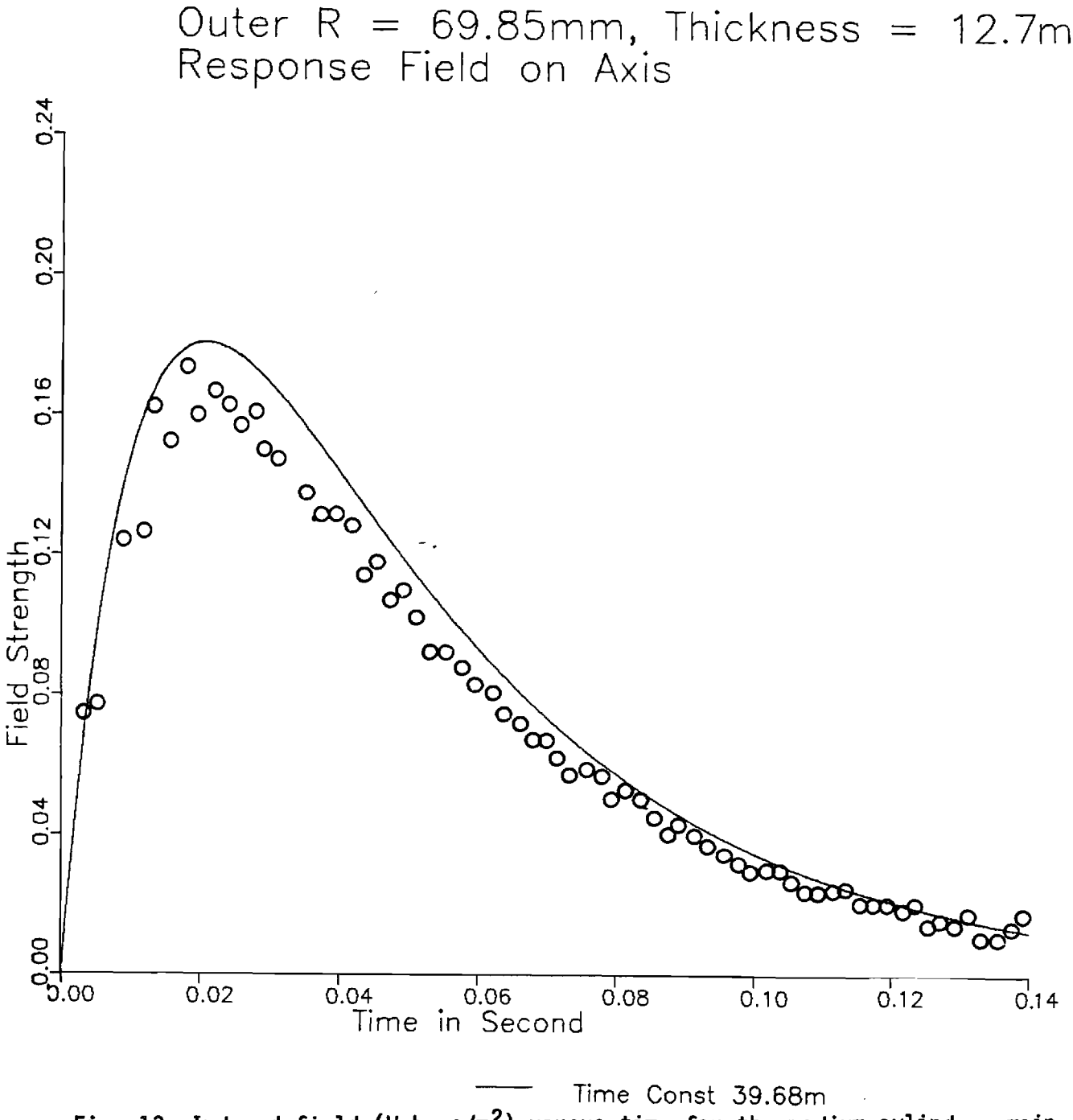

Fig. 13 Induced field (Webers/m^2) versus time for the medium cylinder; main field time constant is 39.68 msec. Dots indicate experimental values 20 cm from the center of the cylinder along the z axis.

Then with $k'^2 = \mu\sigma\lambda$, it follows that

$$\frac{1}{r}\frac{d}{dr}\left(r\frac{dR}{dr}\right) + \left[\left(k'^2 - \ell^2\right) - \frac{m^2}{r^2}\right]R = 0 \tag{35}$$

$$\frac{d^2\theta}{d\theta^2} + m^2\theta = 0 \tag{36}$$

$$\frac{d^2Z}{dz^2} + \ell^2 Z = 0 \tag{37}$$

For our problem meaningful solutions result when $m = 1$, $\ell = n\pi/L$ (i.e., $A \sim \sin\left(\frac{n\pi}{L} z\right)$ where L = total length). From (35) we find a new eigenvalue $k'^2 = k^2 + \ell^2 = k^2 + \left(\frac{n\pi}{L}\right)^2$ with a modified reciprocal time constant $\lambda = \frac{k^2 + (n\pi/L)^2}{\mu\sigma}$. Even for the short cylinder in Felix, the dominant eigenvalues with n = 1 have virtually no length modifications since k is so much larger than π/L.

Discussion and Conclusions

The null field integral technique offers a rather simple method of predicting transient eddy current solutions using small determination matrices. The salient features of the technique revolve around the intelligent choice of interfacial basis functions. These basis functions can be inferred as perturbations from known solutions or from experimental tests. For example, one might conceivably construct a set of basis sets by looking at interfacial field data at t = 0, half way through the process, and near the end of a process.

An extension of the method to the short cylinder considering the 3-D nature of the field can be obtained by constructing the following basis sets for both A_z and A_θ

$$A_z, \frac{\partial A_z}{\partial n} \simeq \sin\theta \cos\frac{\pi}{L} z \tag{38}$$

$$A_\theta, \frac{\partial A_\theta}{\partial n} \simeq \cos\theta \sin\frac{\pi}{L} z \tag{39}$$

where z = 0 is set at the midpoint (L/2) on the cylinder. Using these basis functions will necessitate the construction of an (8 x 8) determination matrix rather than the (4 x 4) used above. Of course, odd multiples of $(\frac{\pi}{L})$ can be used, but these only yield higher order perturbations to the base system eigenvalues.

REFERENCES

[1] W. F. Praeg, et al., "Felix, An Experimental Facility to Study Electromagnetic Effects for First Wall, Blanket, and Shield Systems," Proc. 9th Symp. on Engineering Problems in Fusion Research, IEEE Pub. No. 81, Ch. 1715, pp. 1763-1766, 1981.

[2] L. R. Turner, et al., "Felix Construction Status and Experimental Program," Nucl. Technol./Fusion, Vol. 4, No. 2, Pt. 2, pp. 745-750, 1983.

[3] L. R. Turner, et al., "Results from the Felix Experiments on Electromagnetic Effects in Hollow Cylinders," Fifth Compumag Conference, Fort Collins, Colorado, pp. 356-359, 1985.

[4] S. Zhi-ming, et al., "The Finite Element Solution of Transient Axi Symmetrical Nonlinear Eddy Current Field Problems," Fifth Compumag Conference, Fort Collins, Colorado, pp. 241-244, 1985.

[5] B. Aldefeld, "A Numerical Solution of Transient Nonlinear Eddy Current Problems Including Moving Iron Parts," IEEE Trans. Magnetics, Vol. MAG-14, No. 5, pp. 371-373, 1978.

[6] A. Kameari and Y. Suzuki, "Eddy Current Analysis by the Finite Element Circuit Method," 7th Symposium, Knoxville, Tennessee, pp. 1386-1392.

[7] S. Tandon, A. Armor, and M. V. K. Chan, "Nonlinear Transient Finite Element Field Computation for Electrical Machines and Devices," IEEE Trans. Power App. Sys., Vol. PAS-102, pp. 1089-1096, May 1983.